

Interpretable cytometry cell-type annotation with flow-based deep generative models.

Quentin Blampey^{1,2}, Nadège Bercovici^{2,3}, Charles-Antoine Dutertre^{2,4}, Isabelle Pic²,
Fabrice André², Joana Mourato Ribeiro², and Paul-Henry Cournède¹

¹Paris-Saclay University, CentraleSupélec, Laboratory of Mathematics and Computer Science (MICS), Gif-sur-Yvette, 91190 France

²Paris-Saclay University, Gustave Roussy, INSERM U981, PRISM Center, Villejuif, France

³Université Paris Cité, Institut Cochin, INSERM, CNRS, Paris, 75014 France

⁴Institut National de la Santé Et de la Recherche Médicale (INSERM) U1015, Equipe Labellisée—Ligue Nationale contre le Cancer, Villejuif, France

August 12, 2022

Abstract

Cytometry enables precise single-cell phenotyping within heterogeneous populations. These cell types are traditionally annotated via manual gating, but this method suffers from a lack of reproducibility and sensitivity to batch-effect. Also, the most recent cytometers — spectral flow or mass cytometers — create rich and high-dimensional data whose analysis via manual gating becomes challenging and time-consuming. To tackle these limitations, we introduce Scyan¹, a Single-cell Cytometry Annotation Network that automatically annotates cell types using only prior expert knowledge about the cytometry panel. We demonstrate that Scyan significantly outperforms the related state-of-the-art models on multiple public datasets while being faster and interpretable. In addition, Scyan overcomes several complementary tasks such as batch-effect removal, debarcoding, and population discovery. Overall, this model accelerates and eases cell population characterisation, quantification, and discovery in cytometry.

1 Introduction

The simultaneous detection of several cellular proteins by spectral and mass cytometry opens up an unprecedented way to detect, quantify, and monitor the function of highly specific cell populations from complex biological samples[1]. These rich analyses are made possible with the usage of large panels of markers, typically more than 30 or 40 markers, which considerably increases the information contained inside the data[2]. They provide key insights to better understand specific diseases, immune cell functions, or monitor the response to therapies[3]. To obtain such results, population annotation must be performed to provide each cell with a biologically meaningful cell type. Yet, due to the data’s high dimensionality and complexity, manual annotations become challenging and labour intensive[4]. This process, called gating[5], is highly subjective and sensitive to the batch effect, or non-biological data variability[4]. These drawbacks are amplified as the number of cytometry samples increases, reinforcing the need to develop and use automatic tools in population annotation and data analysis[6, 7].

¹<https://github.com/MICS-Lab/scyan>

Many unsupervised clustering tools[8, 9, 10] have been developed for automatic data exploration and population discovery. However, a manual analysis of marker expressions is still required to name each cluster with a meaningful cell type. Indeed, clusters do not necessarily correspond to one specific cell type, and it is up to the investigator to decide which population each cluster corresponds to. For this reason, tools that directly annotate populations are more appropriate when one must obtain population annotations. The first category of annotation models are supervised or semi-supervised models[11, 12, 13], which rely on prior manual gating of large datasets to train the models. Moreover, these models are also limited to populations that were already labelled. The second category, to which our model belongs, are unsupervised annotation models that leverage prior biological knowledge about the panel of markers. Although some models have been developed[14, 15, 13], they either (i) lack interpretability, (ii) can not discover new populations, (iii) require the usage of batch-effect correction models before being applied, or (iv) scale poorly to large datasets. Another consideration is how Deep Learning has been underused for cytometry annotations, a type of model that has proven efficient and flexible for many related work in various domains of applications[16, 17, 18].

In this paper, we introduce a single-cell cytometry annotation network called Scyan that annotates cell types and corrects batch effects concurrently, without any label or gating needed. Scyan is a Bayesian probabilistic model composed of a deep invertible neural network called a normalizing flow[19, 20, 21]. This flow transforms cell data into a latent space that is used for annotation, does not contain batch effect, and is key for population discovery.

We also demonstrate Scyan efficiency, scalability, and interpretability on multiple public mass cytometry datasets for which manually annotated cell populations are considered ground truth. We compare Scyan classification performance to other knowledge-based approaches[14, 15] and with a clustering-based semi-supervised method[8, 14]. Additionally, we illustrate batch-effect correction on one of the above datasets, and we show that our model can be used

for population discovery, as well as for the general task of debarcoding. These properties make Scyan an end-to-end analysis framework for mass cytometry and (spectral) flow cytometry.

2 Results

2.1 Scyan model architecture

Multiparametric cytometry, such as mass cytometry or spectral flow cytometry, allows measuring dozens of protein expressions on single cells. Scyan is a deep generative model (Figure 1) that can integrate and analyse these data. It is composed of a neural mapping f_ϕ (Figure 1b) between observed multidimensional marker expressions and latent marker expressions. We model the latent expressions by the sum of a cell-specific term (for instance resulting from autofluorescence) and a population-specific term obtained from expert knowledge about the cytometry panel. This expert knowledge has the form of a table (Figure 1a) that contains meaningful values to describe the expected expression of one marker for one population, typically: - (negative expression), + (positive expression), intermediate values like "mid" and "low", or "not applicable".

The model's latent space is designed to be free of batch effect and unified for all markers. Each component of the latent expression typically varies between -1 and 1, representing respectively negative and positive expressions for a specific marker. All latent markers have similar expression ranges, making the latent space biologically meaningful and easy to interpret.

The latent distribution is a mixture of distributions, each being associated with exactly one population. This distribution mixture only depends on the biological knowledge that the user provides and is used to annotate cell types based on the Bayes rule. This is done after mapping marker expressions into the latent space via f_ϕ , which is a deep neural network composed of several elementary units called coupling layers (Figure 1c). Each of these units is invertible, making f_ϕ also invertible, so that we can transform a measured cell expression vec-

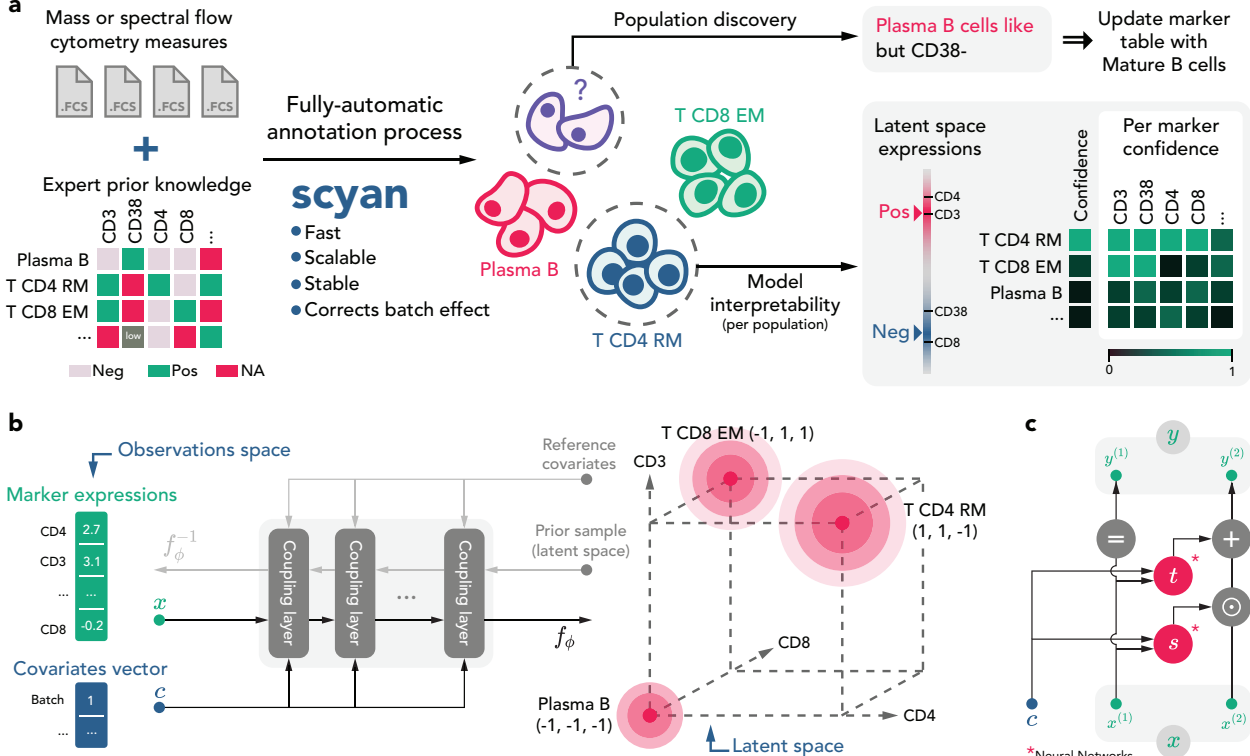


Figure 1: **Overview of Scyan usage and architecture.** **a**, Illustration of Scyan typical use case. It requires one or multiple cytometry acquisitions and a marker table that details which population is expected to express which markers. Then, Scyan annotates cells in a fast and unsupervised (or fully-automatic) manner while removing batch effect (if any). We then provide interpretability tools to understand Scyan annotations and discover new populations that can eventually be added to the table afterwards. **b**, Scyan is composed of a neural network f_ϕ that maps observed expressions into latent expressions. The latent space can be seen as a mixture of Gaussian-like distributions on the vertices of a hypercube. **c**, One coupling layer, the elementary unit that composes the transformation f_ϕ , contains two multi-layer perceptrons (s and t) and uses cell covariates such as the batch information.

tor \mathbf{x} into a latent expression vector \mathbf{u} and reciprocally. This kind of transformation, called normalizing flows[19, 20, 21], can be used to compute the exact likelihood of data samples, which is essential for annotations.

2.2 Multitask benchmark on public datasets

Classification metrics comparison We compare Scyan to the related works on public mass cytometry datasets collected from healthy bone marrow. One is from patients with acute myeloid leukemia[8] (AML, $N = 104\,184$ cells) and the other from bone marrow mononuclear cells[22] (BMMC, N

$= 61\,725$ cells). For the AML dataset, we use 14 markers of the panel to identify 14 populations, while for the BMMC dataset, we use 13 markers to identify 19 populations. Manual gating has been performed in previous studies[8, 22], providing ground truth labels to evaluate annotation models. Note that the unsupervised models listed below do not use these labels during training.

We compared Scyan to three other knowledge-based models: ACDC[14], the baseline of ACDC, and MP[15]. Also, we compared our model to a semi-supervised approach based on Phenograph[8] clustering. Note that the Phenograph clustering does not predict labels itself, thus each cluster is associated with a population in a semi-supervised way, i.e., us-

ing some of the labels. Because it uses true labels, the Phenograph-based model could have an advantage in the annotation task. We evaluated the models using accuracy, macro averaged F1-score, and balanced accuracy. The results are summarized in Table 1 and illustrated in Figure 2.

The tests show that Scyan outperforms the other models. In particular, Scyan is about 20 points higher than the other models on BMMC for the F1-score and the balanced accuracy, which is explained by the capacity of Scyan to better detect small populations (Figure 2a). Ten sub-populations represent less than one per cent of the total number of cells, making these populations more difficult to detect and label. Yet, small population annotations can still be essential, and thus so is Scyan’s capacity to detect them.

Computational Speed and Scalability To demonstrate the scalability of Scyan on large datasets, using SMOTE[23, 24] we oversample cells from the AML dataset to millions of cells and compare the execution times of the different algorithms (Figure 3a). All experiments were run using the same hardware; in our case, CPUs only (i.e. no GPU acceleration). On $N = 10^5$ cells, Scyan runs in less than two minutes, while ACDC and MP need half an hour to one hour. As we increase the number of cells (until $N = 1.6 \cdot 10^6$), the computation times of MP and ACDC reach one day, while Scyan can be trained in approximately four minutes. Scyan scales well to large datasets, as shown by the low slope on Figure 3a. This decreasing slope is explained by the fact that it learns a transformation over a space of size M (the number of markers) instead of directly learning a specific annotation for each cell. Thus, while the number of cells increases, the spatial complexity does not, and the model remains fast to train. If Scyan is set up to correct batch effect, its training time increases but remains comparable to the default Scyan running time — 6 minutes instead of 4 on $N = 1.6 \cdot 10^6$ cells — which is more than two orders of magnitude faster than ACDC and MP.

Scyan corrects batch effect concurrently to annotations A batch effect is a phenomenon that

induces data variability due to non-biological factors such as the use of a different antibody or slightly different cytometer settings. In practice, these factors may introduce variability that interferes with the analysis and can lead to confusion, over-interpretation, and difficulties in annotating populations. To tackle this issue, Scyan can make some corrections to align the inter-batch distributions. Classically, batch effect correction is performed before annotation, but our method allows for correcting it at the same time as the annotation. We illustrate Scyan’s ability to correct batch effect on the AML dataset, for which we have the presence of two batches (H1 with 72 463 cells and H2 with 31 721 cells). We show that Scyan successfully aligned the distributions from both batches (Figure 3b). Note that we used a UMAP[25] to plot cells on a two-dimensional space, but any other dimension reduction tool such as a t-SNE[26] can be used.

Scyan allows for using covariates associated with each cell as inputs of its neural network, which can help condition the latent distributions and thus remove potential confounding factors. This property is also used to correct batch effect. The batch information can indeed be used as the conditioning covariate. During the annotation learning process, Scyan corrects the batch effect by overlapping the inter-batch distributions on its latent space according to a chosen reference batch. We typically choose the batch reference for its representativeness and its large number of cells. As the network is invertible, we can map each cell from the latent space (in which there is no batch effect) to the original space as if all cells came from the reference batch. Thus, we do not need to fit a UMAP reducer again after batch effect removal because Scyan transforms latent cells back into the original space, i.e. where the dimension reduction was performed. This property is particularly suitable for large datasets whose UMAP or t-SNE computation is time-consuming. Thus, being able to reuse a trained dimension reducer accelerates visualisation at each new sample acquisition.

Scyan can perform barcoding deconvolution Barcoding is a method that reduces the batch ef-

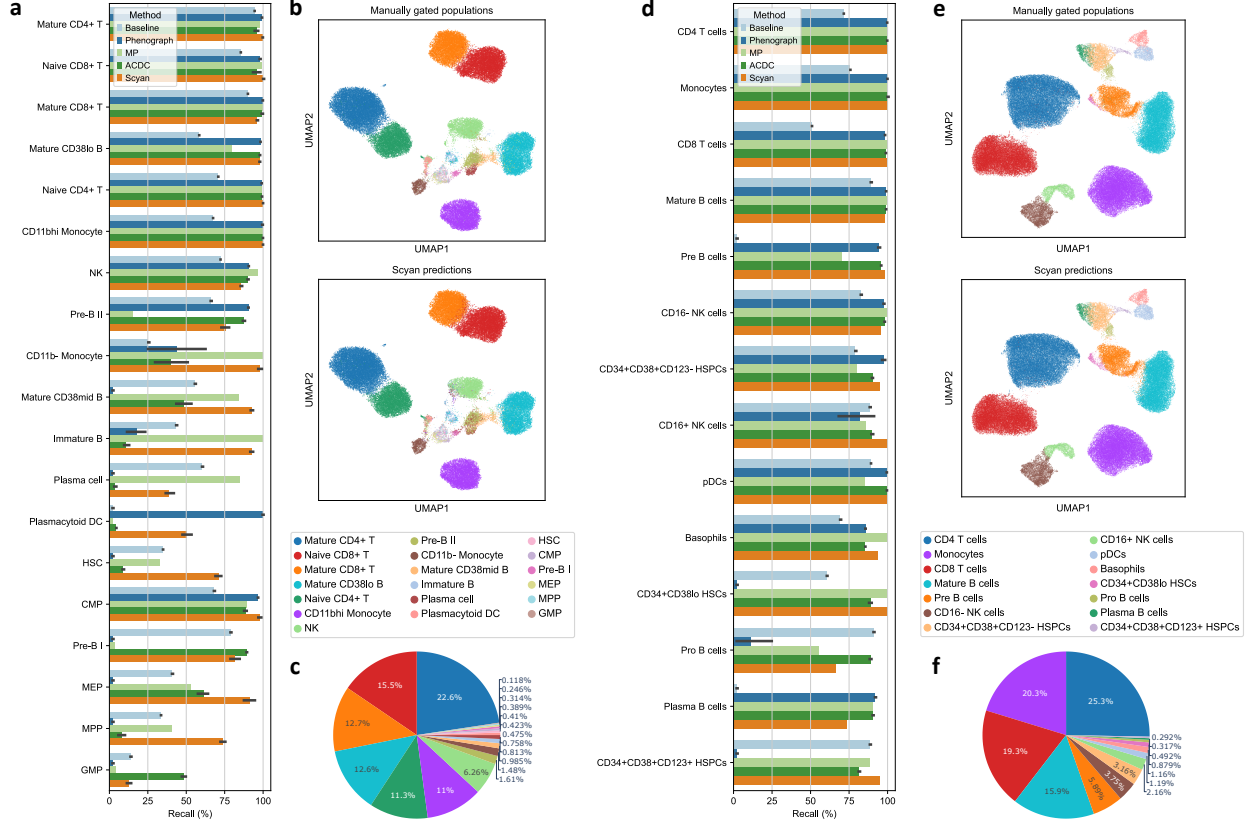


Figure 2: Comparison of Scyan performance on BMMC (a, b, c — on the left) and AML (d, e, f — on the right). a, d. Fraction of cells that were retrieved (recall) for each population and for each method. The considered methods are a Phenograph-based[8] semi-supervised model and four knowledge-based approaches: ACDC[14], its baseline, MP[15] and Scyan (ours). **b, e.** Comparison of the considered ground truth annotation (top) and Scyan annotations (bottom) plotted on a two-dimension UMAP[25]. **c, f.** Proportion of each cell population.

fect and data variability by allowing the processing of multiple cell samples together, each cell sample being labelled — or barcoded — with a unique combination of antibodies (Figure 3c). This protocol requires (i) the dedication of a few markers to make barcodes and (ii) the identification of each cell sample based on its barcode. The latter task, called debarcoding[27], can also be expressed as a knowledge-based annotation task. In this situation, we annotate samples instead of populations, and the expert knowledge required for this task simply corresponds to the known barcodes. As illustrated in Figure 3c/d/e, we demonstrate that Scyan can be successfully applied to debarcoding on a public dataset with 20 barcodes and 6 markers[27].

We added two barcodes corresponding to only negative and only positive markers, with the objective to filter these cells before further analysis. The UMAP on Figure 3e shows a clear separation of the different barcodes, with some small residual clusters (not to be considered) corresponding to complete positive or complete negative barcodes. On Figure 3d, we can see that we retrieve the first four marker expressions of the five chosen barcodes from Figure 3c, demonstrating that Scyan was able to efficiently perform debarcoding.

Table 1: Model performance summary on the AML and BMMC datasets. Apart from Phenograph, no model requires training labels, and we use manual gating annotations as ground truth to compute the metrics. Standard deviations were computed on 20 runs with different seeds and are written with a \pm . *Phenograph-based model with semi-supervision to provide a cell type to each cluster.

	Baseline	Phenograph*	MP	ACDC	Scyan (ours)
BMMC					
Accuracy (%)	77.1	93.7 \pm 0.7	93.4	93.0 \pm 1.0	96.7 \pm 0.2
Balanced accuracy (%)	55.8	54.3 \pm 2.5	67.4	62.1 \pm 1.5	81.9 \pm 0.6
F1-Score (%)	57.0	45.9 \pm 2.6	60.0	57.7 \pm 1.5	80.5 \pm 0.9
AML					
Accuracy (%)	68.0	96.8 \pm 0.6	96.7	98.3 \pm 0.0	98.4 \pm 0.3
Balanced accuracy (%)	66.9	75.4 \pm 2.8	89.7	93.4 \pm 0.2	92.3 \pm 3.5
F1-Score (%)	64.3	72.4 \pm 3.1	86.0	85.7 \pm 0.2	91.4 \pm 3.2

2.3 Scyan is a transparent and reliable model

Standard visualisations Providing explanations for the annotations is essential to validate model predictions in the absence of ground truth. A simple yet crucial visualisation tool is obtained with two-dimensional scatter plots, i.e. all cells scattered on a graph whose dimensions correspond to two markers expressions. Usually, investigators choose markers that are discriminative toward some populations. Although they do not capture the full complexity of data, combining multiple scatter plots can be very informative. We use them to visualise each population annotated by Scyan, and we offer the possibility to let Scyan choose the most discriminative markers automatically for the scatter plots. We applied these visualisations to the BMMC dataset, with a focus on B cells. In Figure 4a, we show that B cells were separated into five populations: Mature CD38low B, Mature CD38mid B, Pre-B I, Pre-B II, and Immature B. Three markers (CD38, CD20, and CD34) were chosen to separate the different populations. While one scatter plot cannot separate these populations, the combination of the three pairwise scatter plots made it possible and readable.

Model interpretability Scyan latent space is key for annotation interpretability. It opens up a new simple way to understand which marker is positive or negative at a glance. Indeed, the latent space is unified for all markers, and expression levels are

indicated by a simple scale between -1 and 1. To interpret Scyan predictions, we can thus display the latent expressions of all populations in one graph (Figure 4b). We can also choose one population, for instance, Mature CD38low B cells, and display marker expressions for this specific population (Figure 4c). We see that, according to Scyan, Mature CD38low B cells are CD20+, CD45+, CD19+, CD4-, CD8-, CD3-, CD34-, CD38-, and CD33-, as intended by the provided knowledge table (Figure 4d). Moreover, the Figure 4b provides information about the markers that were not part of the knowledge table for this population; for instance, Scyan found that these Mature CD38low B cells were CD45+ and CD45RA+ (note that CD45 was marked as NA in the table, but we could write "+").

Another consideration is how humanly readable the Scyan annotation process is. We can select a cell type and detail why Scyan predicted this cell type and not another one. Indeed, instead of predicting just one population for each cell, Scyan predicts an array of probabilities for all potential populations for each cell. Each population is associated with a confidence, and each population-confidence is decomposed into a sum of log probabilities for each marker (Figure 4e). These population-marker log probabilities show which marker reduced the confidence associated with a population. To target more cells, we average Scyan confidence over a group of cells or over a cell type; for instance, on Figure 4e, Mature CD38low B cells were selected. As previously seen in Figure 4c,

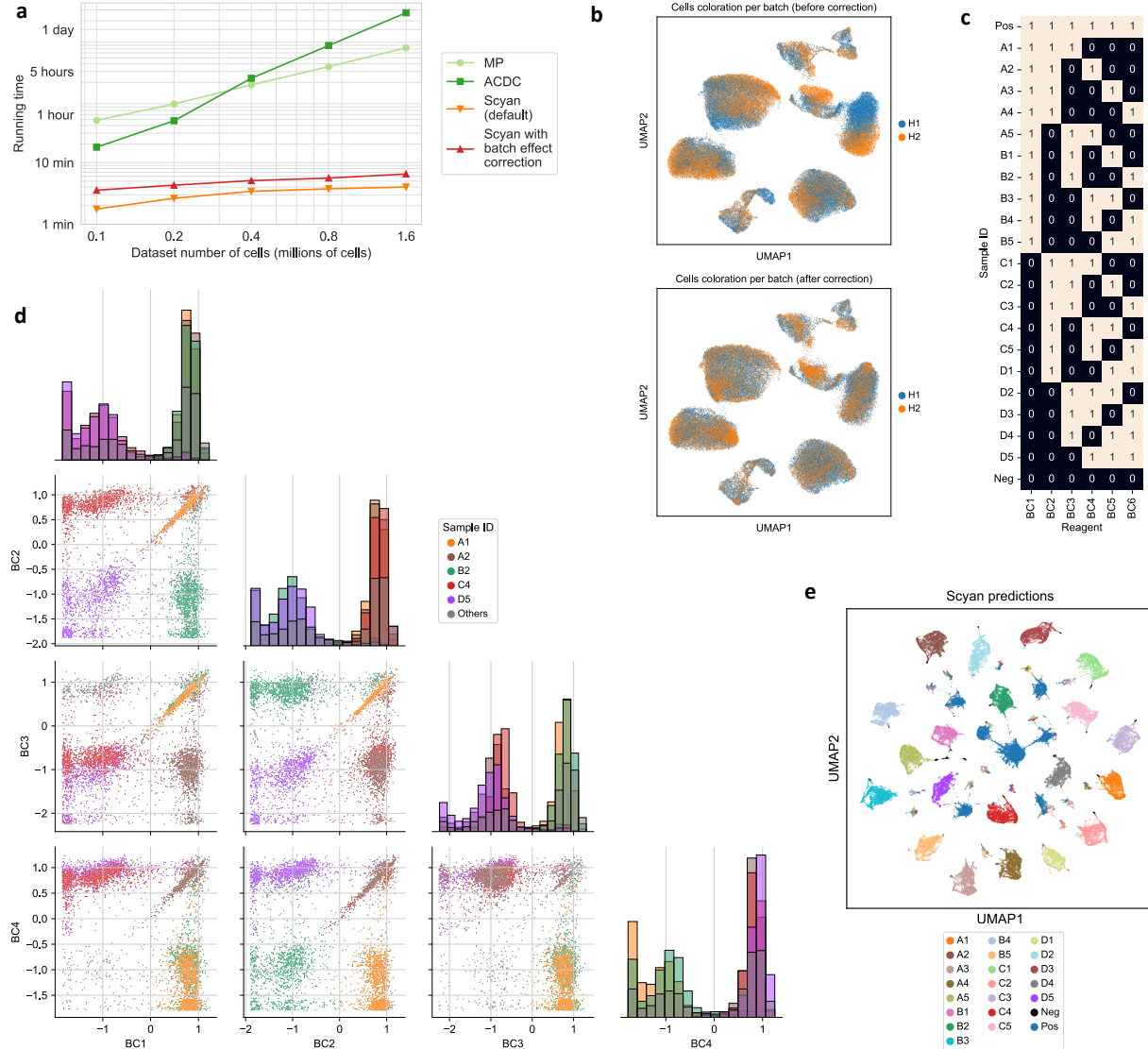


Figure 3: Illustration of Scyan scalability and ability to correct batch effect or retrieve barcodes. **a**, Runtime comparison on multiple dataset sizes (obtained by oversampling) for MP, ACDC and Scyan (ours). **b**, Batch-effect correction performed by Scyan on the AML dataset. The two batches are displayed before correction (top) and after prediction/correction (bottom). **c**, List of all barcodes considered for the debarcoding task (22 samples and 6 markers). **d**, Visualisation of 5 predicted barcodes for the first three markers of the barcode dataset (standardised marker expressions). **e**, Scyan predictions on the barcode dataset displayed on a two-dimensional UMAP.

Mature CD38low B cells are CD38low / neg. This specificity decreased the probability of these cells being predicted as Mature CD38mid B cells, as can be seen on the second row and second to last column

of Figure 4e. The next population on the list was Immature B, which was not predicted because of the high expression of CD20. These plots rely on the usage of biological knowledge, which makes the Scyan

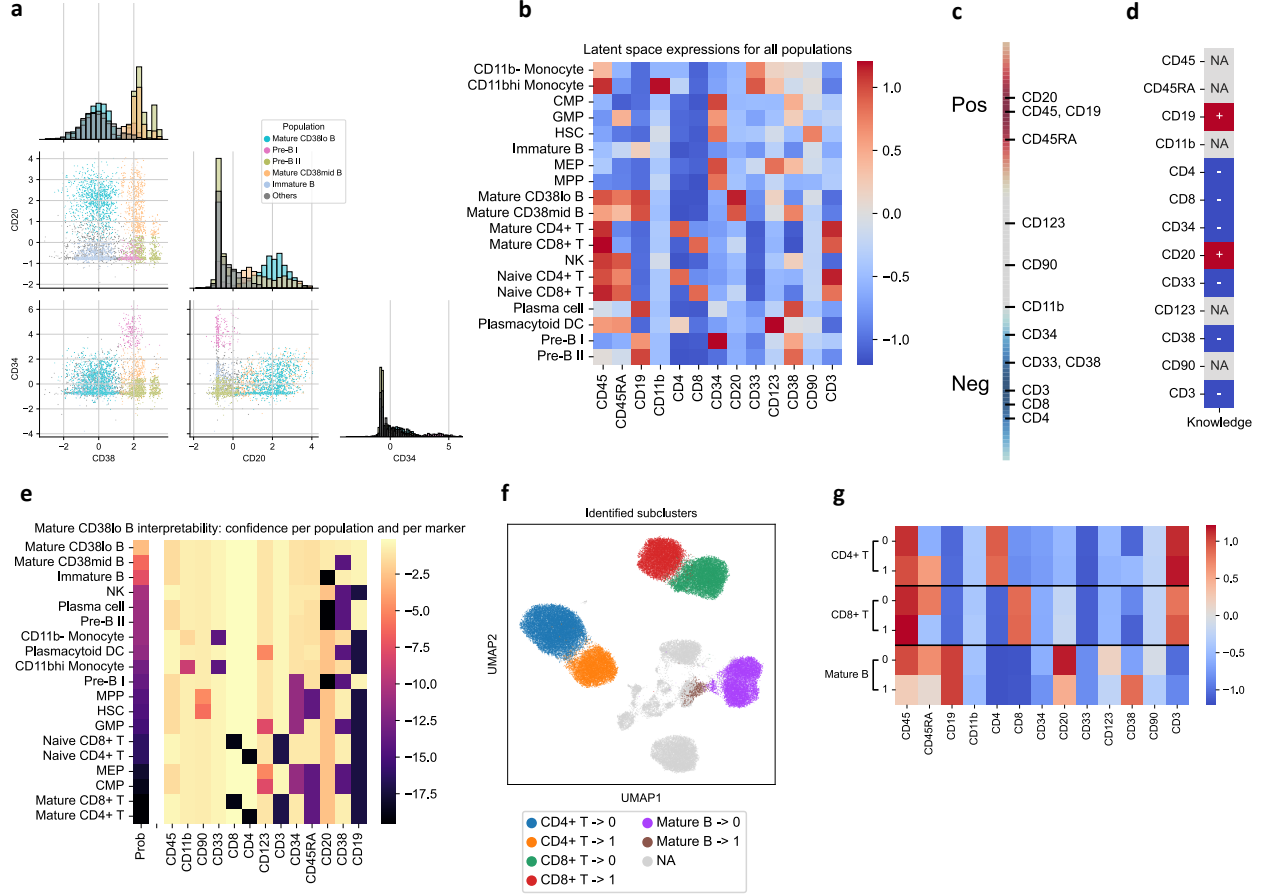


Figure 4: **Scyan visualisation, interpretability, and discovery on BMMC.** **a**, Separation of all the B cell populations on multiple scatter plots using CD38, CD20, and CD34 (standardised marker expressions). **b**, Scyan latent space for all populations. The latent space comprises one value per marker whose typical range is [-1, 1]. The closer to -1, the more negative the marker expression, and the closer to 1, the more positive the marker expression. **c**, Scyan latent space for Mature CD38-low B cells; in other words, their expression for all the considered markers. **d**, Extract of the knowledge table concerning Mature CD38-low B cells. Some markers were known to be positive, others negative, and some marker expressions were unknown or not applicable (NA). **e**, Understanding Scyan predictions for Mature CD38-low B cells by providing Scyan confidence (or probability) for each population, each them decomposed per marker. **f**, Sub-clusters identified for population discovery. Some populations were separated into multiple clusters that we can further analyse (see g), while some populations are already precise enough (NA). **g**, Mean latent expression of cells in each cluster identified in (f) for population discovery. Based on the CD45RA expressions, we can retrieve Mature CD4 T, Naive CD4 T, Mature CD8 T and Naive CD8 T cells. Based on the CD38 expressions, we retrieve Mature CD38lo B and Mature CD38mid B cells.

annotation process interpretable.

2.4 Enhancing annotations with population discovery

One apparent limitation of knowledge-based annotation models is that predictions are limited to populations from the provided table. For this rea-

son, we provide tools to possibly identify new sub-populations that are not considered in the table. Again, we base our population discovery approach on Scyan latent space. Each population is decomposed into multiple sub-clusters (Figure 4f), which can be explored and analysed on Scyan latent space (Figure 4g). It provides a way to distinguish small new sub-clusters by highlighting which markers vary

between them. One key asset of our approach is that we can also use markers for which we have no prior knowledge (NA markers) to identify these sub-clusters. Then, if a sub-cluster corresponds to a biologically-meaningful population, it can be added to the marker-population table. It allows us to go deeper into the sub-populations and, in the end, be able to understand the full diversity of the cell types from the cytometry samples.

We illustrate population discovery on the BMMC dataset. For this purpose, we remove some knowledge about the characterisation of six populations from the table and show that we can retrieve the missing knowledge. More specifically, instead of considering Mature CD4 T cells and Naive CD4 T cells, we gather the two populations together as CD4 T cells in the table and remove the knowledge about CD45RA. Indeed, Mature CD4 T cells are CD45RA- while Naive CD4 T cells are CD45RA+. Similarly, we merge Naive and Mature CD8 T cells into CD8 T cells (we remove knowledge about CD45RA), and we also merge Mature CD38-low B and Mature CD38-mid B into Mature B (we remove knowledge about CD38). In Figure 4f/g, we show that we successfully retrieve the missing sub-populations by providing two sub-clusters for CD4 T cells, CD8 T cells and Mature B cells. Analysing the differential marker expression between these sub-clusters allows for characterising more refined sub-populations in the table. The six sub-clusters correspond to the population names we removed, and once the clusters were named, these new cell annotations match 98.2% of the ground truth labels. The abovementioned approach shows that we can start by analysing large populations and gradually infusing the discovered populations into the table to refine the results.

3 Discussion

We have introduced Scyan, a multitask neural network for cytometry annotation, batch-effect removal, debarcoding, and population discovery. It provides a robust and broad pipeline to analyse cytometry cell populations, monitor their dynamics over time, and compare the populations proportions among pa-

tients. Such analyses are key to projects that aim to discover biomarkers or specific populations responsible for some treatments' success. The number of these projects grows while aggregating bigger and bigger datasets with dozens or hundreds of samples. Scyan can perform fast and automatic annotations for these large datasets and correct some potential batch effects. Some studies reduce this batch effect with barcoding, which requires a debarcoding step that Scyan can also perform. Thus, Scyan is suitable for many tasks and many cytometry projects, and does not rely on any extra cytometry analysis library. In particular, it can directly take new cytometry files and evolve simultaneously with a study by readjusting its parameters at each new acquisition to provide population characterisation and quantification in real-time.

Scyan annotates populations without needing labels and therefore does not rely on manual gating. Instead, it uses a marker-population table containing expert knowledge. The literature offers many resources and existing knowledge to construct such a table, but some marker expressions remain unexplored. For this reason, we offer the possibility to handle "not applicable" values inside the table and, to improve flexibility, intermediate expressions such as "mid" or "low". In the case where the panel remains not well known enough to build the input table, Scyan can help discover new populations: analyses start by annotating large populations and then gradually target smaller and smaller cell types. Also, with the increasing usage of cytometry, we expect the marker knowledge to improve over time, reinforcing Scyan performance and ease of use.

In terms of model architecture, normalizing flows are a recent and promising field of research in generative models. They benefit from interesting mathematical properties such as (i) exact likelihood computation and (ii) invertibility. We show that normalizing flows can be used to leverage marker knowledge in a biologically natural way, providing interpretability. Indeed, the network invertibility allows switching between the measured marker expressions and their latent expressions. In this space, all latent markers have unified expression ranges, which is convenient for human analysis, especially for population discov-

ery. It also make the model reliable and transparent to biologists, which can build trust toward the model annotations and validate them. Moreover, normalizing flows are smooth transformations that control how the space is deformed, ensuring that we do not alter the biological meaning behind marker expressions. At the same time, it benefits from the expressiveness and flexibility of deep neural networks. In fact, the usage of neural networks allows adding additional terms in the loss function to handle the batch effect, which is naturally corrected with the network invertibility. Eventually, we can further push the usage of these convenient mathematical properties for other tasks in single-cell analysis, for instance, single-cell RNA sequencing data or imaging mass cytometry data[28].

4 Methods

4.1 Scyan model

In this section, we formulate the annotation problem and detail the Scyan model illustrated in Figure 1b/c. Let $\mathbf{x}_1, \dots, \mathbf{x}_N \in \mathbb{R}^M$ represent the vectors of M marker expressions for N cells. We assume these expression levels have already been transformed using the *asinh* or *logicle*[29] transformation, and standardised. Our objective is to associate each cell to one of the P predefined cell types using a marker-population table $\rho \in \mathbb{R}^{P \times M}$, with $\rho_{z,m}$ summarising the knowledge about the expression of marker m for the population z . If it is known that population z expresses m then $\rho_{z,m} = 1$; if we know that it does not express m then $\rho_{z,m} = -1$. Otherwise, if we have no knowledge or if the expression can vary among the population, then $\rho_{z,m} = \text{NA}$. Note that it is also possible to choose values in \mathbb{R} ; for instance, for mid or low expressions, we can choose 0 and 0.5 respectively (see Supplemental section 7). In addition, we can add covariates $\mathbf{c}_1, \dots, \mathbf{c}_N \in \mathbb{R}^{M_c}$ associated to each cell, e.g. information about the batch or which antibody has been used by the cytometer. M_c denotes the number of covariates; it can be zero if no covariate is provided.

Generative process Let \mathbf{X} be the random vector of size M representing one cell by its standardised marker expressions; in other words, \mathbf{X} is the random variable from which $\mathbf{x}_1, \dots, \mathbf{x}_N$ are sampled. We model \mathbf{X} by the following deep generative process:

$$\begin{aligned} Z &\sim \text{Categorical}(\boldsymbol{\pi}) \\ \mathbf{E} \mid Z = (e_m)_{1 \leq m \leq M}, \text{ where } \begin{cases} e_m = \rho_{Z,m} & \text{if } \rho_{Z,m} \neq \text{NA} \\ e_m \sim \mathcal{U}([-1, 1]) & \text{otherwise,} \end{cases} \\ \mathbf{H} &\sim \mathcal{N}(\mathbf{0}, \sigma \mathbf{I}_M) \\ \mathbf{U} &= \mathbf{E} + \mathbf{H} \\ \mathbf{X} &= f_\phi^{-1}(\mathbf{U}). \end{aligned} \tag{1}$$

In the above equations, $\boldsymbol{\pi} = (\pi_z)_{1 \leq z \leq P}$ represents the weights of each population, with the constraints $\pi_z \geq 0$ and $\sum_z \pi_z = 1$. Z is the random variable corresponding to a cell type among the P possible ones. \mathbf{E} is a population-specific variable whose terms are either known according to the expert knowledge table ρ or drawn from a uniform distribution between negative expressions (represented by -1) and positive expressions (represented by +1). \mathbf{H} contains cell-specific terms, such as autofluorescence. Finally, \mathbf{U} is the cell's latent expressions, summing a population-specific component and a cell-specific one. Also, \mathbf{U} can be transformed into a measured cell marker expressions vector \mathbf{X} by the inverse of a deep invertible network f_ϕ detailed below.

Invertible transformation network The core network, f_ϕ (illustrated in Figure 1b), is a normalizing flow[19, 20, 21]. It transforms the target distribution p_X into the known base distribution p_U which was described in the previous section. Using a change of variables, we can compute the exact likelihood of a sample \mathbf{x} by:

$$p_X(\mathbf{x}; \boldsymbol{\theta}) = p_U(f_\phi(\mathbf{x}); \boldsymbol{\pi}) \cdot \log \left| \det \frac{\partial f_\phi(\mathbf{x})}{\partial \mathbf{x}^T} \right|. \tag{2}$$

To be able to compute this expression, we need to choose an invertible network with a tractable Jacobian determinant. We have chosen a set of transformations called Real Non-Volume-Preserving (Real NVP[30]) transformations, which are compositions of

functions, named coupling layers $f_\phi := f^{(L)} \circ f^{(L-1)} \circ \dots \circ f^{(1)}$ with L the number of coupling layers. Each coupling layer $f^{(i)} : (\mathbf{x}, \mathbf{c}) \mapsto \mathbf{y}$ splits both \mathbf{x} and \mathbf{y} into two components $(\mathbf{x}^{(1)}, \mathbf{x}^{(2)}), (\mathbf{y}^{(1)}, \mathbf{y}^{(2)})$ on which distinct transformations are applied. We propose below an extension of the traditional coupling layer[30] to integrate covariates \mathbf{c} (illustrated in Figure 1c):

$$\begin{cases} \mathbf{y}^{(1)} = \mathbf{x}^{(1)} \\ \mathbf{y}^{(2)} = \mathbf{x}^{(2)} \odot \exp(s([\mathbf{x}^{(1)}; \mathbf{c}])) + t([\mathbf{x}^{(1)}; \mathbf{c}]). \end{cases} \quad (3)$$

In the equations above, \odot stands for the element-wise product, $[.;.]$ is the concatenation operator, and (s, t) are functions from \mathbb{R}^{d+M_c} to \mathbb{R}^{M-d} where d is the size of $\mathbf{x}^{(1)}$. These functions can be arbitrarily complex, in our case, multi-layer-perceptrons. Note that the indices used by the coupling layer to split \mathbf{x} into $(\mathbf{x}^{(1)}, \mathbf{x}^{(2)})$ are set before training and are different for every coupling layer. This way, we ensure that the flow transforms all the markers. Each coupling layer has an easy-to-compute log Jacobian determinant, which is $\sum_i s([\mathbf{x}^{(1)}; \mathbf{c}])_i$, and is easily invertible as shown in the following equations:

$$\begin{cases} \mathbf{x}^{(1)} = \mathbf{y}^{(1)} \\ \mathbf{x}^{(2)} = (\mathbf{y}^{(2)} - t([\mathbf{y}^{(1)}; \mathbf{c}])) \odot \exp(-s([\mathbf{y}^{(1)}; \mathbf{c}])). \end{cases} \quad (4)$$

As f_ϕ is a stack of coupling layers, it is also invertible, and its log Jacobian determinant is obtained by summing each coupling layer log Jacobian determinant. Stacking many coupling layers is essential to learning a rich target distribution and complex variables interdependencies.

Learning process The model parameters are $\theta = (\pi, \phi)$. For computational stability during training, instead of learning π itself we actually learn logits $(l_z)_{1 \leq z \leq P}$ from which we obtain $\pi_z = \frac{e^{l_z}}{\sum_k e^{l_k}}$. By doing this, we ensure the positivity of each weight and guarantee they sum to 1. To train the model, we minimise the Kullback–Leibler (KL) divergence between the cell’s empirical marker-expression distribu-

tion p_{X^*} and our model distribution p_X . It is equivalent to minimising the negative log-likelihood of the observed cell expressions $-\mathbb{E}_{\mathbf{x} \sim p_{X^*}} [\log p_X(\mathbf{x}; \theta)]$ over θ . Using Equation 2 and adapting it to integrate covariates leads to minimising the following quantity:

$$\mathcal{L}_{KL}(\theta) = - \sum_{1 \leq i \leq N} \left[\log(p_U(f_\phi(\mathbf{x}_i, \mathbf{c}_i); \pi)) + \log \left| \det \frac{\partial f_\phi(\mathbf{x}_i, \mathbf{c}_i)}{\partial \mathbf{x}^T} \right| \right]. \quad (5)$$

In the above equation, $p_U(f_\phi(\mathbf{x}_i, \mathbf{c}_i); \pi) = \sum_{z=1}^P \pi_z \cdot p_{U|Z=z}(f_\phi(\mathbf{x}_i, \mathbf{c}_i))$, which is not computationally tractable because the presence of NA in ρ leads to the summation of a uniform and a normal random variable. We approximate the density of the sum of the two random variables by a piecewise density function that is constant on $[-1 + \sigma, 1 - \sigma]$ with Gaussian queues outside of this interval. In practice, we choose a normal law with a low standard deviation, which leads to a good piecewise approximation (see Supplemental section 7). If we consider the KL-divergence as described above, some modes may collapse; that is, one small population may not be predicted. Indeed, a small population z that has a small weight π_z leads to smaller gradients towards this population. To solve this issue, we favour small populations once every two epochs. For that, for all z , we replace π_z by $\pi_z^{(-T)} = \frac{e^{-l_z/T}}{\sum_k e^{-l_k/T}}$ where T is called temperature[31, 32] as it increases the entropy of $\pi^{(-T)}$. Note that here we added the minus signs to reverse the weights of the populations so that it favours small ones. A temperature close to 0 leads to high weights for small populations, while an infinite temperature leads to equal population weights, i.e., the maximum entropy. Alternating between π and $\pi^{(-T)}$ allows for a better balance of population sizes at the end of the training.

We also add a maximum mean discrepancy (MMD[33]) term to align the distributions from every batch b in the latent space so that it is free of batch effect. Formally, we add $\mathcal{L}_B(\theta) = \sum_{b \neq \text{ref}} \mathcal{MMD}(\mathbf{u}_{1:\mathbf{W}}^{\text{ref}}, \mathbf{u}_{1:\mathbf{W}}^b)$, where $\mathbf{u}_{1:\mathbf{W}}^{\text{ref}}$ and $\mathbf{u}_{1:\mathbf{W}}^b$ are \mathbf{W} latent cells from the chosen reference batch ref and batch b respectively. That is, we pass a mini-batch of B cells $\mathbf{x}_{1:B}^{\text{ref}}, \mathbf{x}_{1:B}^b$ through f_ϕ to get

$\mathbf{u}_{1:B}^{ref}, \mathbf{u}_{1:B}^b$. Then, we perform a weighted sampling of W latent cells among the B latent cells; their weights depend on their predicted population, i.e., if Scyan predicts the population z for the latent cell \mathbf{u}_i^b then its associated weight is $1/\pi_z$. Thus, we expect to sample a similar amount of cells from every population.

The complete loss is obtained by a weighted sum of the two losses described above: $\mathcal{L}(\theta) = \mathcal{L}_{KL}(\theta) + \alpha \cdot \mathcal{L}_B(\theta)$, where α is set to have comparable losses values. We optimize the complete loss on mini-batches of cells using the Adam optimizer[34]. Once finished training, the annotation process \mathcal{A}_θ consists in choosing the most likely population according to the data using Bayes's rule. So, for a cell \mathbf{x} with covariates \mathbf{c} , we have:

$$\mathcal{A}_\theta(\mathbf{x}, \mathbf{c}) = \arg \max_{1 \leq z \leq P} \pi_z \cdot p_{U|Z=z}(f_\phi(\mathbf{x}, \mathbf{c})). \quad (6)$$

4.2 Batch-effect correction on dimension reduction plots

We designed the loss function such that the latent space is free of batch effect. Using this property, combined with the network invertibility, enables batch-effect correction. To effectively correct the batch effect of a sample \mathbf{x} with covariates $\mathbf{c} \neq \mathbf{c}_{ref}$, we first transform \mathbf{x} into its latent expressions via f_ϕ . Since the latent space is batch-effect free, latent expressions can then be transformed back into the original space using the covariates of the reference batch and f_ϕ^{-1} . Formally, we denote by $\tilde{\mathbf{x}}$ the batch-effect corrected cell associated to \mathbf{x} ; that is, $\tilde{\mathbf{x}} = f_\phi^{-1}(f_\phi(\mathbf{x}, \mathbf{c}), \mathbf{c}_{ref})$. In this manner, we get expressions $\tilde{\mathbf{x}}$ as if \mathbf{x} were cell expressions from the reference batch. Thus, the latent space is used to align the distributions in the original space. Note that, since batch-effect was corrected in the original space, it is possible to reuse a trained dimension reduction tool (e.g., a UMAP). Applying this UMAP again does not change the dimension reduction of the cells from the reference (due to the network invertibility), but it updates those of all the other batches.

4.3 Interpretability and population discovery

Latent expressions Scyan interpretability is based on its latent space. Considering a cell \mathbf{x} and its covariates \mathbf{c} , its latent representation is $\mathbf{u} = f_\phi(\mathbf{x}, \mathbf{c})$. The information of which marker is positive or negative is contained in \mathbf{u} . Indeed, $u_m \approx 1$ corresponds to a positive expression, while $u_m \approx -1$ represents a negative expression, whatever the marker m (i.e., expression levels for all markers are unified). Similarly, $u_m \approx 0$ is a mid-expression, and so on. We average the latent cell expressions over one population to obtain a latent expression at the population level. These population-level latent expressions can be displayed for one population (Figure 4c) or for all of them at once (Figure 4b).

Differential expressions for population discovery We extend this interpretability tool for population discovery. We first perform a Leiden clustering[9] over all the cells with a high resolution to get a large number of clusters. Then, we use this clustering to separate each predicted population into multiple sub-clusters. Each sub-cluster can then be explored using the previously described latent space, showing exactly where the differences between each sub-cluster are. On Figure 4g, the model automatically fills unknown expressions (NA in the table) since the latent space represents expressions for all markers. Also, if some markers of the panels are entirely unknown, they can still be added inside the marker-population table as a column of "NA". Even though such a marker does not provide much information for the prediction, it can be very informative for population discovery as it will thus appear in the heatmap. Also, note that some clusters appear as "NA" in Figure 4f. They correspond to sub-clusters that were not significant enough according to a threshold in terms of ratio of cells. If too few clusters are displayed, one can increase the resolution to obtain more clusters.

Understanding Scyan predictions Additionally, $U_1 | (Z = z), \dots, U_M | (Z = z)$ are independent for every population z . It means that we can decompose $\log p_{U|Z=z}(\mathbf{u}) = \sum_m \log p_{U_m|Z=z}(u_m)$, and

we can gather all these terms into a matrix of scores $(\log p_{U_m|Z=z}(u_m))_{z,m}$. The term $\log p_{U_m|Z=z}(u_m)$ can be interpreted as the impact of marker m towards the prediction of the population z for the latent cell expression \mathbf{u} . Based on that, we can interpret Scyan predictions for a group of cells $(\mathbf{x}_i, \mathbf{c}_i)_i$ by transforming the cells into their latent expressions and then averaging the score matrices. The resulting matrix is typically displayed on a heatmap (Figure 4e), and populations are sorted by their score (sum over a score matrix row). Note that, in the figure, each population score is scaled to make it easier to read.

Automatic scatter plots We automatically choose a set of very discriminative markers to enhance two-dimensional scatter plots (Figure 4a). For that, let K be the number of markers requested by the user. For each marker of the panel, we compute the sum of the Kolmogorov-Smirnov test for every population of interest in a "one-versus-all" manner (the user also chooses the populations of interest). Each marker has its own statistic, and we choose the K first markers whose statistics are the highest.

4.4 Model hyperparameter optimisation

One important issue in training deep learning models is fine-tuning their hyperparameters. Because our model is unsupervised, we cannot consider any supervised metric such as accuracy. We thus have to use an unsupervised metric that measures the annotation quality. For this reason, we defined a heuristic that combines (i) a clustering metric, the Davies-Bouldin Index[35] (DBI), to obtain well-separated clusters, (ii) a count of the missing populations to favour the presence of all populations among the predictions, and (iii) a Dirichlet probability on population weights to favour population diversity. Formally, let O be the number of populations that the model did not predict at all, and $\mathbf{X}, \mathbf{y}_{pred}$ the cells' expressions and predictions, respectively. Then, we define our heuristic to be minimised by $(O + 1) \cdot DBI(\mathbf{X}, \mathbf{y}_{pred}) \cdot (-\sum_z \log \pi_z)$. Note that the last term is proportional to the log Dirichlet probability of the learned

population weights π . An advantage of using the DBI is that it is computationally more efficient than some clustering metrics, such as the silhouette score[36]. In particular, the DBI scales efficiently to large datasets.

4.5 Preprocessing and implementation details

Data preprocessing To compare our model with the other methods, we used a similar data preprocessing, and the same knowledge tables as MP[15] and ACDC[14] for both the AML and BMMC datasets. Due to the impossibility of having non-binary values in the input tables of MP and ACDC, some cell types could not be described by their tables and were removed. For a fair comparison, we did not consider these cell types either. Also, ACDC and MP used $x \mapsto \text{asinh}(\frac{x-1}{5})$ to preprocess marker expressions, which we reused. Note that we also standardised the data (required to run Scyan). Concerning the debarcoding task, we used the logicle transformation[29] to preprocess marker expressions and then standardisation.

Implementation details We implemented our model using Python and the Deep Learning framework Pytorch[37]. We used between 6 and 8 coupling layers whose multi-layer-perceptrons (s, t) have each between 6 and 8 hidden layers depending on hyperparameter optimisation. Concerning the MMD, we automatically chose the Gaussian kernel bandwidth with the median heuristic[38]. In particular, the typical bandwidth corresponds to the expected median squared distance of two i.i.d samples from H , that is, $2\sigma^2 \cdot (M - 2)$. In practice, we simply used $2\sigma^2 M$, which corresponds to the mean of the squared distances. We reused this bandwidth with different scales to obtain a multi-scale kernel. Moreover, the metrics used for the performance benchmark were those of Scikit-Learn[39].

5 Acknowledgement

This work is supported by Prism – National Precision Medicine Center in Oncology funded by the France

2030 programme and the French National Research Agency (ANR) under grant number ANR-18-IBHU-0002.

6 Data availability

The three datasets and knowledge tables considered in this paper are public and accessible at https://github.com/MICS-Lab/scyan_data

References

- [1] Behbehani, G. K. Immunophenotyping by Mass Cytometry. *Methods Mol Biol* 2032, 31–51 (2019).
- [2] Spitzer, M. H. & Nolan, G. P. Mass Cytometry: Single Cells, Many Features. *Cell* 165, 780–791 (2016).
- [3] McKinnon, K. M. Flow Cytometry: An Overview. *Curr Protoc Immunol* 120, 5.1.1–5.1.11 (2018).
- [4] Newell, E. W. & Cheng, Y. Mass cytometry: blessed with the curse of dimensionality. *Nat Immunol* 17, 890–895 (2016).
- [5] Staats, J., Divekar, A., McCoy, J. & Maecker, H. Guidelines for Gating Flow Cytometry Data for Immunological Assays. in *Methods in molecular biology* (Clifton, N.J.) vol. 2032 81–104 (2019).
- [6] Newell, E. W. & Cheng, Y. Mass cytometry: blessed with the curse of dimensionality. *Nat Immunol* 17, 890–895 (2016).
- [7] Aghaeepour, N. et al. Critical assessment of automated flow cytometry data analysis techniques. *Nat Methods* 10, 228–238 (2013).
- [8] Levine, J. H. et al. Data-Driven Phenotypic Dissection of AML Reveals Progenitor-like Cells that Correlate with Prognosis. *Cell* 162, 184–197 (2015).
- [9] Traag, V. A., Waltman, L. & van Eck, N. J. From Louvain to Leiden: guaranteeing well-connected communities. *Sci Rep* 9, 5233 (2019).
- [10] Qiu, P. et al. Extracting a cellular hierarchy from high-dimensional cytometry data with SPADE. *Nat Biotechnol* 29, 886–891 (2011).
- [11] Li, H. et al. Gating mass cytometry data by deep learning. *Bioinformatics* 33, 3423–3430 (2017).
- [12] Abdelaal, T. et al. Predicting Cell Populations in Single Cell Mass Cytometry Data. *Cytometry Part A* 95, 769–781 (2019).
- [13] Liu, P. et al. Recent Advances in Computer-Assisted Algorithms for Cell Subtype Identification of Cytometry Data. *Front Cell Dev Biol* 8, 234 (2020).
- [14] Lee, H.-C., Kosoy, R., Becker, C. E., Dudley, J. T. & Kidd, B. A. Automated cell type discovery and classification through knowledge transfer. *Bioinformatics* 33, 1689–1695 (2017).
- [15] Ji, D., Nalisnick, E., Qian, Y., Scheuermann, R. H. & Smyth, P. Bayesian Trees for Automated Cytometry Data Analysis. in *Proceedings of the 3rd Machine Learning for Healthcare Conference* 465–483 (PMLR, 2018).
- [16] Lopez, R., Regier, J., Cole, M. B., Jordan, M. I. & Yosef, N. Deep generative modeling for single-cell transcriptomics. *Nat Methods* 15, 1053–1058 (2018).
- [17] Zhang, A. W. et al. Probabilistic cell-type assignment of single-cell RNA-seq for tumor microenvironment profiling. *Nat Methods* 16, 1007–1015 (2019).
- [18] Amodio, M. et al. Exploring single-cell data with deep multitasking neural networks. *Nat Methods* 16, 1139–1145 (2019).
- [19] Rezende, D. J. & Mohamed, S. Variational Inference with Normalizing Flows. *arXiv:1505.05770 [cs, stat]* (2016).
- [20] Papamakarios, G., Nalisnick, E., Rezende, D. J., Mohamed, S. & Lakshminarayanan, B. Normalizing Flows for Probabilistic Modeling and Inference. *arXiv:1912.02762 [cs, stat]* (2021).

[21] Izmailov, P., Kirichenko, P., Finzi, M. & Wilson, A. G. Semi-Supervised Learning with Normalizing Flows. arXiv:1912.13025 [cs, stat] (2019).

[22] Bendall, S. C. et al. Single-Cell Mass Cytometry of Differential Immune and Drug Responses Across a Human Hematopoietic Continuum. *Science* 332, 687–696 (2011).

[23] Chawla, N. V., Bowyer, K. W., Hall, L. O. & Kegelmeyer, W. P. SMOTE: Synthetic Minority Over-sampling Technique. *jar* 16, 321–357 (2002).

[24] Lemaître, G., Nogueira, F. & Aridas, C. K. Imbalanced-learn: A Python Toolbox to Tackle the Curse of Imbalanced Datasets in Machine Learning. *Journal of Machine Learning Research* 18, 1–5 (2017).

[25] McInnes, L., Healy, J. & Melville, J. UMAP: Uniform Manifold Approximation and Projection for Dimension Reduction. arXiv:1802.03426 [cs, stat] (2020).

[26] van der Maaten, L. & Hinton, G. Vizualizing data using t-SNE. *Journal of Machine Learning Research* 9, 2579–2605 (2008).

[27] Zunder, E. R. et al. Palladium-based mass tag cell barcoding with a doublet-filtering scheme and single-cell deconvolution algorithm. *Nat Protoc* 10, 316–333 (2015).

[28] Chang, Q. et al. Imaging Mass Cytometry. *Cytometry A* 91, 160–169 (2017).

[29] Parks, D. R., Roederer, M. & Moore, W. A. A new “Logicle” display method avoids deceptive effects of logarithmic scaling for low signals and compensated data. *Cytometry Part A* 69A, 541–551 (2006).

[30] Dinh, L., Sohl-Dickstein, J. & Bengio, S. Density estimation using Real NVP. arXiv:1605.08803 [cs, stat] (2017).

[31] Ackley, D. H., Hinton, G. E. & Sejnowski, T. J. A learning algorithm for boltzmann machines. *Cognitive Science* 9, 147–169 (1985).

[32] Ficler, J. & Goldberg, Y. Controlling Linguistic Style Aspects in Neural Language Generation. <http://arxiv.org/abs/1707.02633> (2017) doi:10.48550/arXiv.1707.02633.

[33] Gretton, A., Borgwardt, K. M., Rasch, M. J., Schölkopf, B. & Smola, A. A kernel two-sample test. *J. Mach. Learn. Res.* 13, 723–773 (2012).

[34] Kingma, D. P. & Ba, J. Adam: A Method for Stochastic Optimization. <http://arxiv.org/abs/1412.6980> (2017) doi:10.48550/arXiv.1412.6980.

[35] Davies, D. & Bouldin, D. A Cluster Separation Measure. *Pattern Analysis and Machine Intelligence, IEEE Transactions on PAMI-1*, 224–227 (1979).

[36] Rousseeuw, P. J. Silhouettes: A graphical aid to the interpretation and validation of cluster analysis. *Journal of Computational and Applied Mathematics* 20, 53–65 (1987).

[37] Paszke, A. et al. PyTorch: An Imperative Style, High-Performance Deep Learning Library. <http://arxiv.org/abs/1912.01703> (2019) doi:10.48550/arXiv.1912.01703.

[38] Garreau, D., Jitkrittum, W. & Kanagawa, M. Large sample analysis of the median heuristic. <http://arxiv.org/abs/1707.07269> (2018) doi:10.48550/arXiv.1707.07269.

[39] Pedregosa, F. et al. Scikit-learn: Machine Learning in Python. *J. Mach. Learn. Res.* 12, 2825–2830 (2011).

[40] Goodfellow, I. J. et al. Generative Adversarial Networks. (2014) doi:10.48550/arXiv.1406.2661.

[41] Kingma, D. P. & Welling, M. An Introduction to Variational Autoencoders. *FNT in Machine Learning* 12, 307–392 (2019).

7 Supplementary information

Approach justification and related work In cytometry, when it comes to model the probability

density functions of multidimensional marker expressions, their appearances make it natural to first consider Gaussian Mixture Models (GMM). However, in practice, each component of a GMM estimated from the data may not necessarily map to one population. Indeed, two small populations can be merged into one, and one large population may be split into two components with no interesting biological distinction between them. Also, we would have to annotate each component of the mixture. It could be done manually or using a semi-supervised approach. Yet, as discussed in the introduction, we prefer to use only the knowledge table ρ instead. In terms of deep generative models, there are two main reasons to choose a Real NVP (the normalizing flow architecture) over GANs[40], and VAEs[41]: the flow invertibility and the ability to compute the exact likelihood of a sample. Indeed, the flow invertibility enables a natural and simple way to correct the batch effect by transforming latent expressions back into the original space. Moreover, the ability to compute the exact likelihood of samples makes the annotation straightforward using the Bayes rule and the known base distribution. Another interesting property is that the Real NVP has a triangular Jacobian with positive terms on the diagonal. It enforces the model to diffuse the marker expressions slowly and prevents multiplication by a negative term. Indeed, such smooth transformations are essential to ensure that we do not mix the mapping between a population component and its actual marker expressions density. Also, the Jacobian determinant term in the loss function controls how much the flow dilates volumes in a point neighbourhood. This term thus prevents the collapse of a vast part of the space into a tiny component of the base distribution. From a biological point of view, the Real NVP transformations can be seen as compositions of complex compensations and monotonic transformations learned via deep learning.

Density approximation in the presence of NA Let z be a population and m a marker such that $\rho_{z,m} = \text{NA}$. It leads to $E_m \mid (Z = z) \sim \mathcal{U}([-1, 1])$ and $H_m \sim \mathcal{N}(0, \sigma)$. Thus, $U_m = E_m + H_m$ does not have a simple density expression. We ap-

proximate the probability density function $p_{U_m \mid Z=z}$ by the following function (see Figure 5), where $r = 1 - \sigma$ and $\gamma = \frac{\sigma\sqrt{2\pi}}{2r + \sigma\sqrt{2\pi}}$:

$$\tilde{p}_{U_m \mid Z=z}(u) = \begin{cases} \gamma \cdot \mathcal{N}(u + r; 0, \sigma) & \text{if } u \leq -r \\ \frac{\gamma}{\sigma\sqrt{2\pi}} & \text{if } u \in]-r, r[\\ \gamma \cdot \mathcal{N}(u - r; 0, \sigma) & \text{if } u \geq r. \end{cases} \quad (7)$$

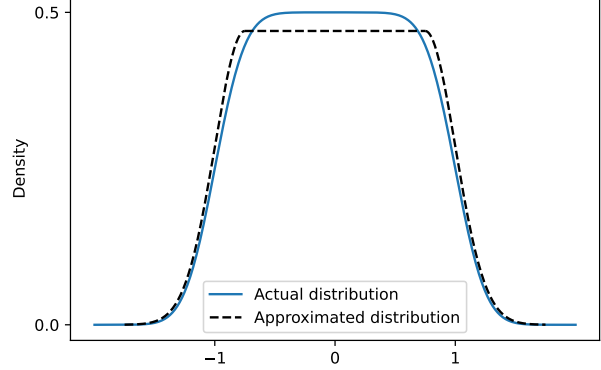


Figure 5: **Density approximation in the presence of NA.** If z and m are a population and a marker respectively such that $\rho_{z,m} = \text{NA}$, then $p_{U_m \mid Z=z}$ is approximated. This figure illustrates the actual and the approximated distribution with $\sigma = \frac{1}{4}$.

Gradients are null in $] -r, r[$, and the queues of the approximated distribution are similar to the actual one. This expression is easy to compute, efficient during training, and a close approximation.

Advice to build the marker-population table
The design of the knowledge table is essential for the annotations. The literature can help its creation, but we also provide some advice to enhance the table:

- It is better to provide no knowledge than false information; therefore, the user should feel comfortable using "Not Applicable" for a marker when unsure. Besides, if needed, population discovery can be used to go deeper into this marker afterwards.
- Note that the model interprets NA values by "any expression is possible". Thus, a population described with extensive use of NA values

Table 2: Models properties comparison. We listed all the models considered in this article as well as manual gating.

	Manual Gating	Baseline	Phenograph	MP	ACDC	Scyan (ours)
Interpretable	X		X	X		X
Reproducible		X	X	X	X	X
Population discovery	X		X		X	X
Soft predictions						X
Generative model						X
Batch-effect correction						X
Continual learning						X

(e.g., above 90% of markers, with no discriminative marker provided) can be over-predicted. This is a normal behaviour since few constraints are applied to this population.

- We enable the usage of intermediate expressions such as "mid" and "low" in the table. Yet, we advise using it only to differentiate two similar populations. Overusing these intermediate expressions in the table will challenge the user to create the table properly while not improving the results.
- It is not required to use all the panel markers. If some markers are unimportant for the annotation, they can be removed from the knowledge table.

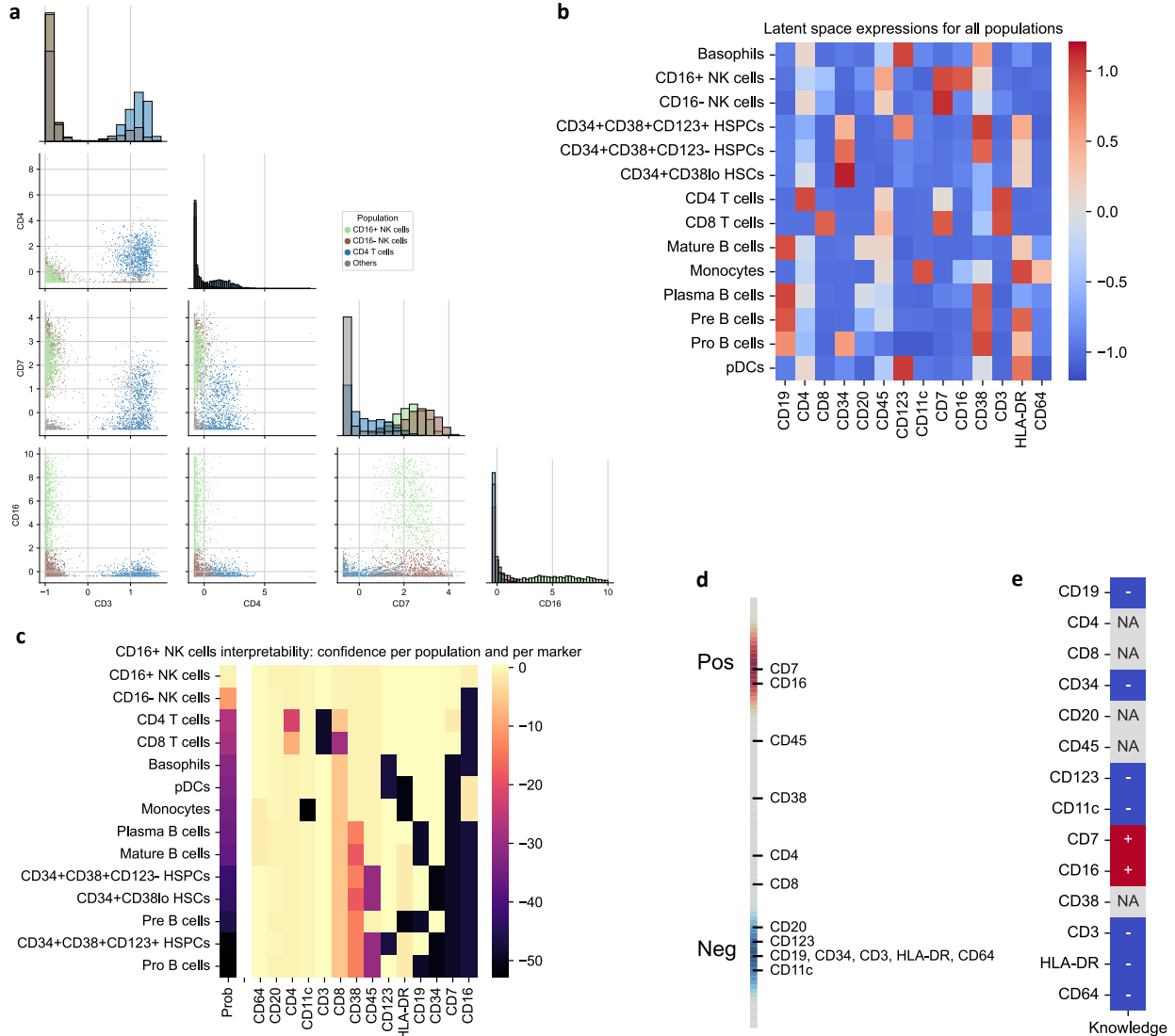


Figure 6: **Scyan visualisation, interpretability, and discovery on AML.** **a**, Separation of the CD4 T cells and the two NK populations on multiple scatter plots using CD3, CD4, CD7 and CD16 (standardised marker expressions). **b**, Scyan latent space for all populations. The latent space comprises one value per marker whose typical range is [-1, 1]. The closer to -1, the more negative the marker expression, and the closer to 1, the more positive the marker expression. **c**, Understanding Scyan predictions for CD16+ NK cells by providing Scyan confidence (or probability) for each population, each of them decomposed per marker. **d**, Scyan latent space for CD16+ NK cells, in other words, their expressions for all the considered markers. **e**, Extract of the knowledge table concerning CD16+ NK cells. Some markers were known to be positive, others negative, and some marker expressions were unknown or not applicable (NA).